



Super Lift Coefficient of Cylinder Using Co-Flow Jet Active Flow Control

Yunchao Yang * Gecheng Zha †
Dept. of Mechanical and Aerospace Engineering
University of Miami, Coral Gables, Florida 33124
E-mail: gzha@miami.edu

Abstract

This paper studies the lift enhancement using Co-Flow Jet (CFJ) active flow control for circular cylinders with Reynolds number of 3×10^6 . For potential flows of a circular cylinder, the maximum lift coefficient limit is derived as 4π . The present study indicates that the zero-net mass-flux CFJ active flow control is able to achieve the maximum lift coefficient that far exceeds the theoretical limit. The present research is based on validated CFD simulation, which employs 2D RANS solver with Spalart-Allmaras (S-A) turbulence model, 5th order WENO scheme for the inviscid fluxes, and 4th order central differencing for the viscous terms. The momentum coefficient C_μ studied is from 0.2 to 0.8 and different CFJ injection and suction slot configurations are varied for parametric trade study. The super-lift coefficient of 28 is obtained at the jet momentum coefficient of $C_\mu = 0.8$. The flow field around the cylinder is attached by the strong circulation between the injection and suction. The stagnation point is detached from the surface by the dramatically increased circulation.

Nomenclature

<i>ESTOL</i>	Extreme Short Take-Off and Landing
<i>AoA</i>	Angle of Attack
<i>AFC</i>	Active Flow Control
<i>CFJ</i>	Co-Flow Jet
<i>FASIP</i>	Flow-Acoustics-Structure Interaction Package
<i>LE</i>	Leading Edge
<i>TE</i>	Trailing Edge
<i>RANS</i>	Reynolds-Averaged Navier-Stokes
<i>ZNMF</i>	Zero-Net Mass Flux
<i>P</i>	CFJ pumping power, $P = \frac{\dot{m}C_p T_{t2}}{\eta} (\Gamma^{\frac{\gamma-1}{\gamma}} - 1)$
η	CFJ pumping system efficiency, propeller efficiency
P_c	Power coefficient, $P_c = \frac{P}{\frac{1}{2}\rho_\infty V_\infty^3 S}$
<i>PR</i>	Total pressure ratio, Γ
C_L	Lift coefficient
C_D	Drag coefficient
C_M	Moment coefficient

* Ph.D. Candidate, AIAA student member

† Professor, ASME Fellow, AIAA associate Fellow

Approved for public release; distribution is unlimited.

C_μ	Jet momentum coefficient, $C_\mu = \frac{\dot{m}V_j}{\frac{1}{2}\rho_\infty V_\infty^2 S}$
C_{Lmax}	Maximum lift coefficient
$(L/D)_c$	Aerodynamic efficiency corrected for CFJ airfoil, $\frac{L}{D+P/V_\infty}$
C_{RW}	Aircraft Productivity parameter
C_L^2/C_D	Productivity efficiency coefficient
$(C_L^2/C_D)_c$	Productivity efficiency coefficient corrected for CFJ airfoil, $(C_L^2/C_D)_c = C_L^2/(C_D + P_c)$
R	Aircraft range
\bar{W}	Aircraft averaged weight during cruise
Re	Reynolds number
M	Mach number
$M_{i,s}$	Isentropic Mach number
C_p	Pressure coefficient
c_p	Constant pressure specific heat
γ	Air specific heats ratio
S	Planform area of the wing
ρ_∞	Freestream density
V_∞	Freestream velocity
T_t	Total temperature
P_t	Total pressure
H_t	Total enthalpy
α	Angle of attack
\dot{m}	Mass flow
C	Chord length
j	Subscript, stands for jet
c	Subscript, stands for corrected

1 Introduction

The flow around a circular cylinder has been studied for fundamental fluid mechanics. The investigation of cylinder flows is of great importance in aerodynamics and engineering applications. Prandtl first studied the lift enhancement by rotating cylinder and concluded that the maximum lift coefficient is 4π from his experiment in 1925 (see Fig. 1) [1]. A rotating cylinder transfers its mechanical energy to the surrounding flow via viscosity with no-slip wall boundary condition. In the early 1920's, the Flettner rotorship was experimented and tested to generate thrust and improve ship efficiency by the Magnus effect. Those pioneering explorations provide some applications of rotating in the cylinder flows.

In classical aerodynamics, the lifting flow over circular cylinder is obtained by superimposing a uniform flow, a doublet and a vortex, which provide the fundamental of lift generation theorem. The flow field is associated with the ratio of rotating speed, which determines the circulation introduced as shown in Fig. 1. The rotating cylinder can be considered the earliest effort of active flow control (AFC) method to achieve lift enhancement. Researchers studied the fluid dynamics and lift and drag coefficient of rotating cylinder [2, 3, 4, 5]. Many researchers applied rotating cylinders in aeronautics [6, 7, 8, 9, 10].

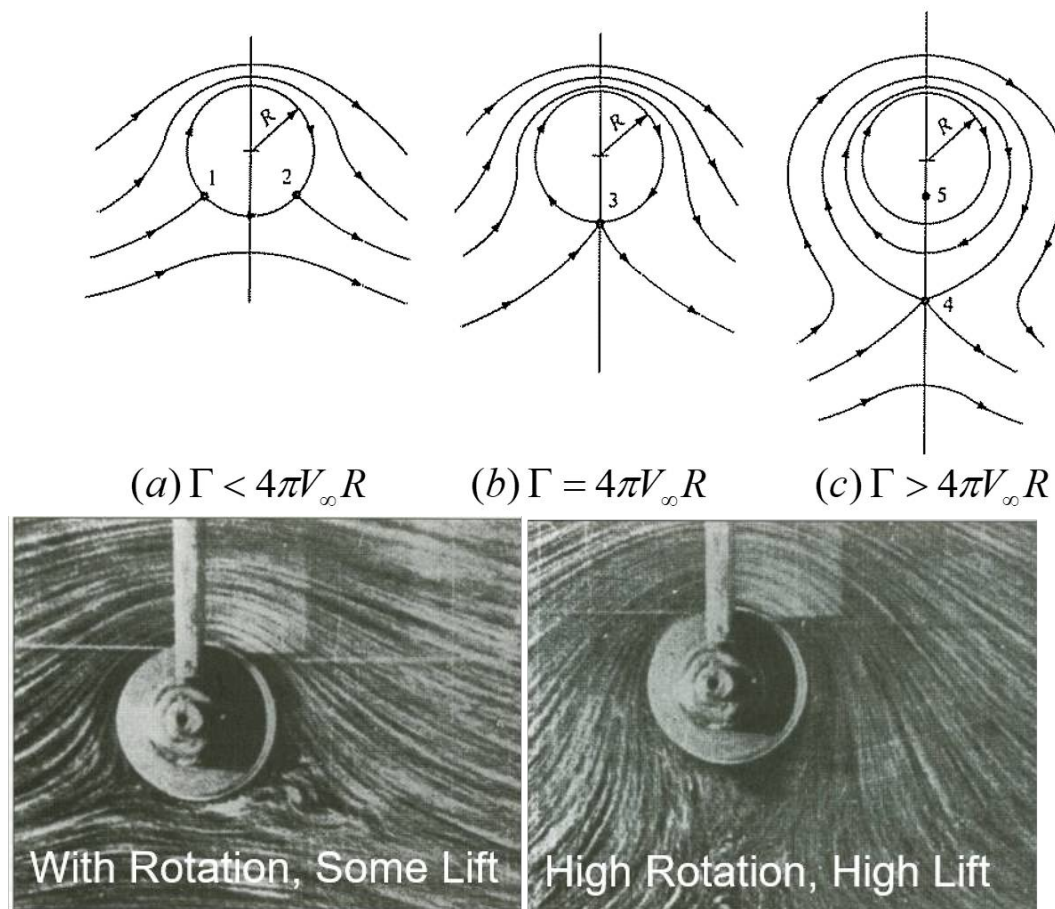


Figure 1: Flow field around a rotating cylinder. (Figures are adapted from reference [11])

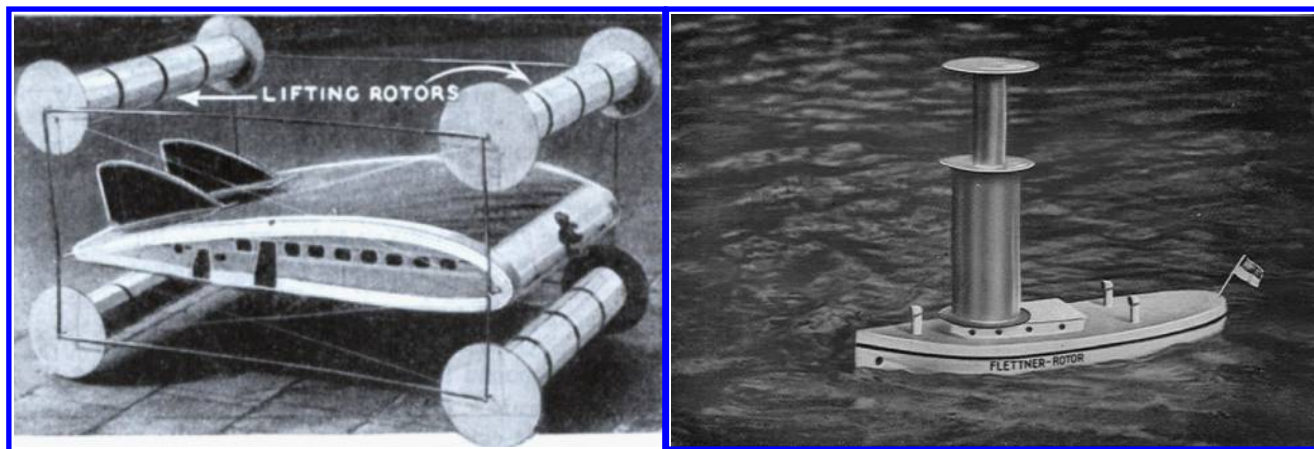


Figure 2: Rotating cylinder application examples, rotor airplane concept(left) and sailing boat(right). (Figures are adapted from [8])

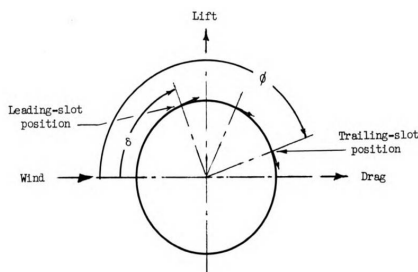


Figure 3: Lifting cylinder using tangential blowing from surface slots.
(Plot is adopted from [12])

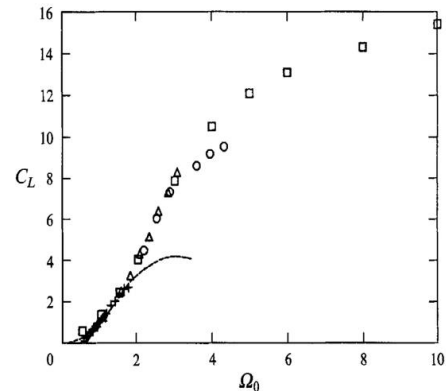
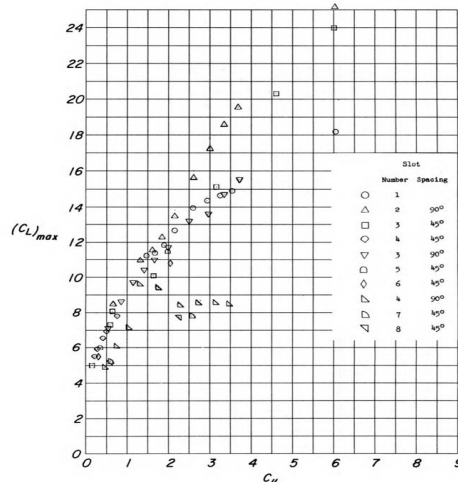


Figure 4: Lift coefficient C_L vs cylinder rotating speed in the rotating cylinder experiment. (Plot is adopted from [2])

Even though Prandtl suggested that the maximum lift coefficient of 4π is the limit for a rotating cylinder if the Kutta condition must be satisfied. Researchers obtained the lift coefficient that exceeds this limit [2, 3]. In 1960s, Lockwood [12] from NASA Langley conducted experiment of a circular cylinder using tangential blowing and achieved the maximum lift coefficient of $C_L \approx 20$ at high blowing jet of $C_\mu \approx 5$ for a very low Reynolds number flow over an end-plated-cylinder with multiple injection slots (See Fig. 4). Tokumaru and Dimotakis in 1993 [2] re-visited the rotating cylinder experiment and obtained the lift coefficient greater than 15 (see Fig. 3).

The rotating cylinder may not be the most effective flow control method to achieve high-lift enhancement, because it requires very large auxiliary energy to rotate a solid cylinder and it is not efficient to transfer the mechanical energy to the flow. Overall, the rotating cylinder and the aforementioned tangential blowing are shown to have very high high energy expenditure.

The recent concept of co-flow jet (CFJ) flow control method, developed by Zha et al. [13, 14, 15, 16, 17, 18, 19, 20, 21, 22, 23] shows a great potential to exceed the lift coefficient limit with high energy efficiency. The CFJ airfoil achieves a dramatically lift augmentation, drag reduction and stall margin increase at low energy expenditure. The purpose of this paper is to apply the CFJ flow control to circular cylinders in order to enhance the lift coefficient at low energy cost. In addition, a cylinder flow can be used as a simple example to study the fundamental fluid mechanics associated with the CFJ flow control.

1.1 The Co-Flow Jet Concept

The CFJ concept was originated for airfoil flow control. The implementation is to open an injection slot near the leading edge(LE) and a suction slot near the trailing edge(TE) on the airfoil suction surface as sketched in Fig. 5. A small amount of mass flow is withdrawn into the airfoil near the TE, pressurized and energized by a pumping system inside the airfoil, and then injected near the LE in the direction tangent to the main flow. The whole process does not add any mass flow to the system and hence is a zero-net mass-flux (ZNMF) flow control. It is a self-contained high lift system with no moving parts.

The fundamental mechanism of the CFJ airfoil is that the turbulent mixing between the jet and main flow energizes the wall boundary-layer, which dramatically increases the circulation, augmenting lift, and reducing

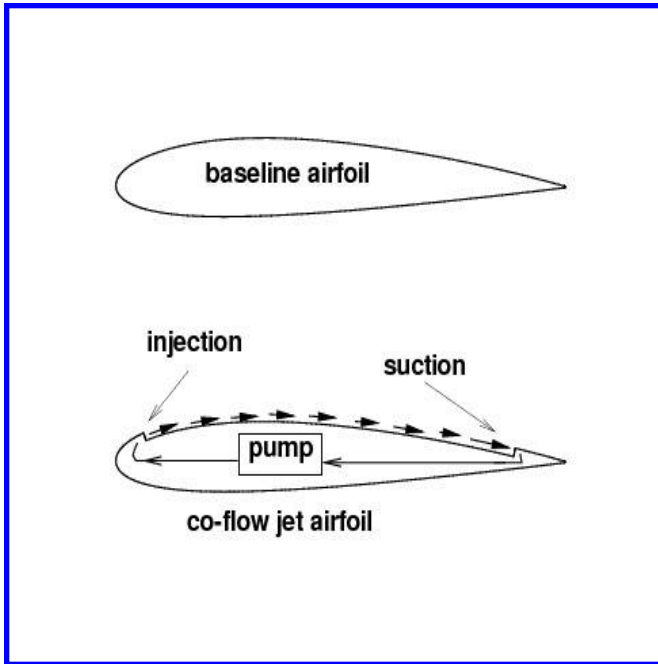


Figure 5: Baseline airfoil and CFJ airfoil.

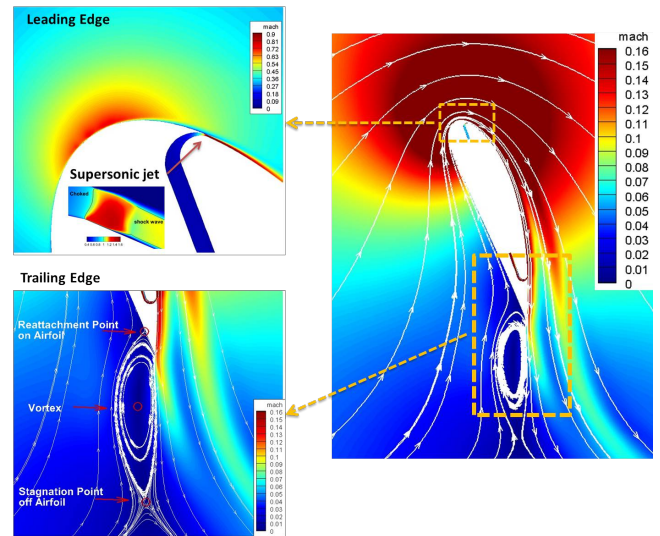


Figure 6: Mach number contours and streamlines at $C_\mu = 0.35$ and $\text{AoA} = 70^\circ$ for the CFJ6421-SST016-SUC053-INJ009 airfoil.

the total drag(or generates thrust) by filling the wake velocity deficit. The CFJ airfoil has a unique low energy expenditure mechanism because the jet gets injected at the leading edge suction peak location, where the main flow pressure is the lowest and makes it easy to eject the flow, and it gets sucked at near the trailing edge, where the main flow pressure is the highest and makes it easy to withdraw the flow.

Fig. 6 from [23] shows the computed flow field of CFJ-NACA6421 airfoil at the AoA of 70° and C_μ of 0.35. The lift coefficient is 10.6, which is greater than the lift limit of 7.6 calculated by Equation (1). The circulation generating the super-lift coefficient is so high that the stagnation point is detached from the airfoil by a large clock-wise vortex beneath the trailing edge. This high momentum jet induction makes the flow attached.

1.2 Objective

The objective of this paper is two folds: 1) to explore the maximum lift coefficient capability of the CFJ flow control on circular cylinder. It is also our interest to study the energy expenditure as compared to the rotating cylinder technique. 2) To conduct parametric study for the CFJ flow control on circular cylinder to identify the optimal injection and suction geometry and jet momentum coefficient

2 CFJ Parameters

This section defines the important parameters to evaluate a CFJ airfoil performance.

2.1 Lift and Drag Calculation

The momentum and pressure at the injection and suction slots produce a reactionary force, which is automatically measured by the force balance in wind tunnel testing. However, for CFD simulation, the full reactionary force needs to be included. Using control volume analysis, the reactionary force can be calculated using the flow parameters at the injection and suction slot opening surfaces. Zha et al. [13] give the following formulations to calculate the lift and drag due to the jet reactionary force for a CFD simulation. By considering the effects of injection and suction jets on the CFJ airfoil, the expressions for these reactionary forces are given as :

$$F_{x_{cfj}} = (\dot{m}_j V_{j1} + p_{j1} A_{j1}) * \cos(\theta_1 - \alpha) - (\dot{m}_j V_{j2} + p_{j2} A_{j2}) * \cos(\theta_2 + \alpha) \quad (1)$$

$$F_{y_{cfj}} = (\dot{m}_{j1} V_{j1} + p_{j1} A_{j1}) * \sin(\theta_1 - \alpha) + (\dot{m}_{j2} V_{j2} + p_{j2} A_{j2}) * \sin(\theta_2 + \alpha) \quad (2)$$

where the subscripts 1 and 2 stand for the injection and suction respectively, and θ_1 and θ_2 are the angles between the injection and suction slot surfaces and a line normal to the airfoil chord. α is the angle of attack.

The total lift and drag on the airfoil can then be expressed as:

$$D = R'_x - F_{x_{cfj}} \quad (3)$$

$$L = R'_y - F_{y_{cfj}} \quad (4)$$

where R'_x and R'_y are the surface integral of pressure and shear stress in x (drag) and y (lift) direction excluding the internal ducts of injection and suction. For the CFD simulation, the total lift and drag are calculated using Eqs. (3) and (4).

2.2 Jet Momentum Coefficient

The jet momentum coefficient C_μ is a parameter used to quantify the injection intensity. It is defined as :

$$C_\mu = \frac{\dot{m} V_j}{\frac{1}{2} \rho_\infty V_\infty^2 S} \quad (5)$$

where \dot{m} is the injection mass flow, V_j the injection velocity, ρ_∞ and V_∞ denote the free stream density and velocity, and S is the platform area.

2.3 Power Coefficient

The CFJ can be implemented by mounting a pumping system inside the wing that withdraws air from the suction slot and blows it into the injection slot. The power consumption can be determined by the jet mass flow and total enthalpy change as the following :

$$P = \dot{m}(H_{t1} - H_{t2}) \quad (6)$$

where H_{t1} and H_{t2} are the total enthalpy in the injection cavity and suction cavity respectively, P is the Power required by the pump and \dot{m} the jet mass flow rate. Introducing the pumping efficiency η and total pressure ratio

of the pump $\Gamma = \frac{P_{t1}}{P_{t2}}$, the power consumption can be expressed as :

$$P = \frac{\dot{m}C_p T_{t2}}{\eta} (\Gamma^{\frac{\gamma-1}{\gamma}} - 1) \quad (7)$$

The power consumption can be expressed as a power coefficient below:

$$P_c = \frac{P}{\frac{1}{2}\rho_\infty V_\infty^3 S} \quad (8)$$

In this research, the pumping efficiency of 100% is used for all the simulations unless indicated otherwise.

2.4 Corrected Aerodynamic Efficiency

The conventional airfoil aerodynamic efficiency is defined as $\frac{L}{D}$. However since CFJ active flow control consumes energy, the CFJ corrected aerodynamic efficiency is modified to take into account the energy consumption of the pump. The formulation of the corrected aerodynamic efficiency for CFJ airfoils is :

$$\left(\frac{L}{D}\right)_c = \frac{L}{D + \frac{P}{V_\infty}} = \frac{C_L}{C_D + P_C} \quad (9)$$

where V_∞ is the free stream velocity, P is the CFJ pumping power, and L and D are the lift and drag generated by the CFJ airfoil. This formulation converts the power consumed by the CFJ into the drag of the airfoil. If the pumping power is set to 0, this formulation returns to the aerodynamic efficiency of a conventional airfoil.

3 Productivity

The transportation ability of an airplane is measured by how much total weight the aircraft can move for the maximum distance. We use a term ‘‘productivity’’ defined as the product of the total weight by the maximum range to represent the transportation ability of an airplane. Even though a cylinder may not be used for aircraft cruise to achieve high productivity, it is still used in this paper as one of the measure of the merits. The following explanation of productivity is hence based on airfoil.

For a jet engine airplane, the total weight of the aircraft decreases during flight. A non-dimensional productivity parameter is hence defined using the aircraft averaged weight as below:

$$C_{RW} = \frac{R\bar{W}}{\frac{1}{2c_t}\bar{\rho}V_\infty^3 S} = \frac{C_L^2}{C_D} \ln \frac{W_0}{W_f} \quad (10)$$

where R is the aircraft range, \bar{W} is the averaged weight of the aircraft during cruise, c_t is the engine cruise thrust specific fuel consumption [fuel weight(N)/(thrust(N) s)], $\bar{\rho}$ is the averaged air density during cruise due to altitude variation, S is the wing platform area, W_0 is the aircraft initial gross weight at takeoff, W_f is the final weight at landing. This formulation is obtained from the Breguet Range Equation. The productivity parameter represents the productivity of the aircraft with the fuel consumed per unit time.

For a propeller engine airplane, the productivity parameter is defined as:

$$C_{RW} = \frac{R\bar{W}}{\frac{1}{2c}\rho V_\infty^2 S} = \eta \frac{C_L^2}{C_D} \ln \frac{W_0}{W_f} \quad (11)$$

where c is the fuel specific consumption of the propeller engine [fuel weight(N)/(BHP(W) s)], η is the propeller efficiency.

For a full electric battery powered propeller airplane, the aircraft weight will not change during flight. The productivity parameter is defined as:

$$C_{RW} = \frac{RW}{\frac{1}{2c}\rho V_\infty^2 S E_c/g} = \eta \frac{C_L^2}{C_D} \frac{W_b}{W_0} \quad (12)$$

where E_c is the battery specific energy density (Wh/kg), W_b is the total battery weight.

To compare aircraft that have the same ratio of initial weight to final weight with the same engine fuel consumption or battery energy density, the only factor affecting their productivity parameter is C_L^2/C_D . We hence name C_L^2/C_D as productivity efficiency.

We consider the productivity efficiency $C_L^2/C_D = C_L(C_L/C_D)$ as a more comprehensive parameter than the conventional aerodynamic efficiency C_L/C_D to measure the merit of an airplane aerodynamic design for cruise performance. The former includes not only the information of C_L/C_D , but also the information of the aircraft weight C_L . For example, for two airplane designs having the same C_L/C_D with one C_L twice larger than the other, if the wing sizes are the same, one airplane will be able to carry twice more weight than the other with productivity and wing loading increased by 100%. Such a large difference is not reflected by C_L/C_D , but very well reflected by C_L^2/C_D .

The definition of C_L/C_D in general is a suitable measure of merit for conventional aircraft design. This is because at a certain Mach number regime, the maximum C_L/C_D is usually achieved at low angle of attack within the drag bucket and is more or less the same for different airfoil designs. In other words, for the same optimum C_L/C_D , the C_L is about the same. A typical C_L for subsonic airfoil is about 0.4 and for transonic airfoil is about 0.7.

For CFJ airfoil, the minimum CFJ pumping power occurs at a fairly high AoA [19, 21]. With the augmentation of CFJ, the subsonic cruise lift coefficient of a CFJ airfoil is typically 2 to 3 times higher than the conventional airfoil with about the same $(C_L/C_D)_c$ [24]. Such a high lift coefficient is unattainable for conventional airfoil since they would be either stalled or near stalled with very high drag. Hence for CFJ aircraft design, the productivity efficiency $C_L^2/C_D = C_L(C_L/C_D)$ is more informative to be used to reflect the aerodynamic performance. The corrected productivity efficiency for CFJ airfoils is $(C_L^2/C_D)_c = C_L^2/(C_D + P_c)$.

4 CFD Simulation Setup

4.1 CFD Code

The in-house FASIP (Flow-Acoustics-Structure Interaction Package) CFD code is used to conduct the numerical simulation. The 2D Reynolds averaged Navier-Stokes (RANS) equations with one-equation Spalart-Allmaras [25] turbulence model is used. A 5th order WENO scheme for the inviscid flux [26, 27, 28, 29, 30, 31] and a 4th order

central differencing for the viscous terms [26, 30] are employed to discretize the Navier-Stokes equations. The low diffusion E-CUSP scheme used as the approximate Riemann solver suggested by Zha et al [27] is utilized with the WENO scheme to evaluate the inviscid fluxes. Implicit time marching method using Gauss-Seidel line relaxation is used to achieve a fast convergence rate [32]. Parallel computing is implemented to save wall clock simulation time [33]. The RANS solver is validated for CFJ airfoil simulations [17, 21, 22, 24, 34, 35].

4.2 Boundary Conditions

The 3rd order accuracy no slip condition is enforced on the solid surface with the wall treatment suggested in [36] to achieve the flux conservation on the wall. Total pressure, total temperature and flow angles are specified as the inlet boundary conditions for the upstream portion of the farfield boundary and inside the injection cavity. Constant static pressure is used for the downstream farfield boundary and inside the suction cavity.

4.3 C_μ Iteration:

To achieve zero net mass flux with the CFJ flow control, the mass flow exiting the injection slot must be equal to the mass flow entering the suction slot, i.e. $\dot{m}_{inj} = \dot{m}_{suc}$. The prescribed jet momentum coefficient C_μ is achieved by adjusting the injection cavity total pressure $P_{t_{inj}}$. Total temperature at the injection is assumed constant during this process. The injection and suction mass flow rates are matched by adjusting the suction cavity static pressure $P_{s_{suc}}$. The iterative process is conducted throughout the simulation until the specified momentum coefficient is reached and the injection and suction mass flow match within the acceptable tolerance, which is 0.2% for the present study.

4.4 Geometry and Mesh

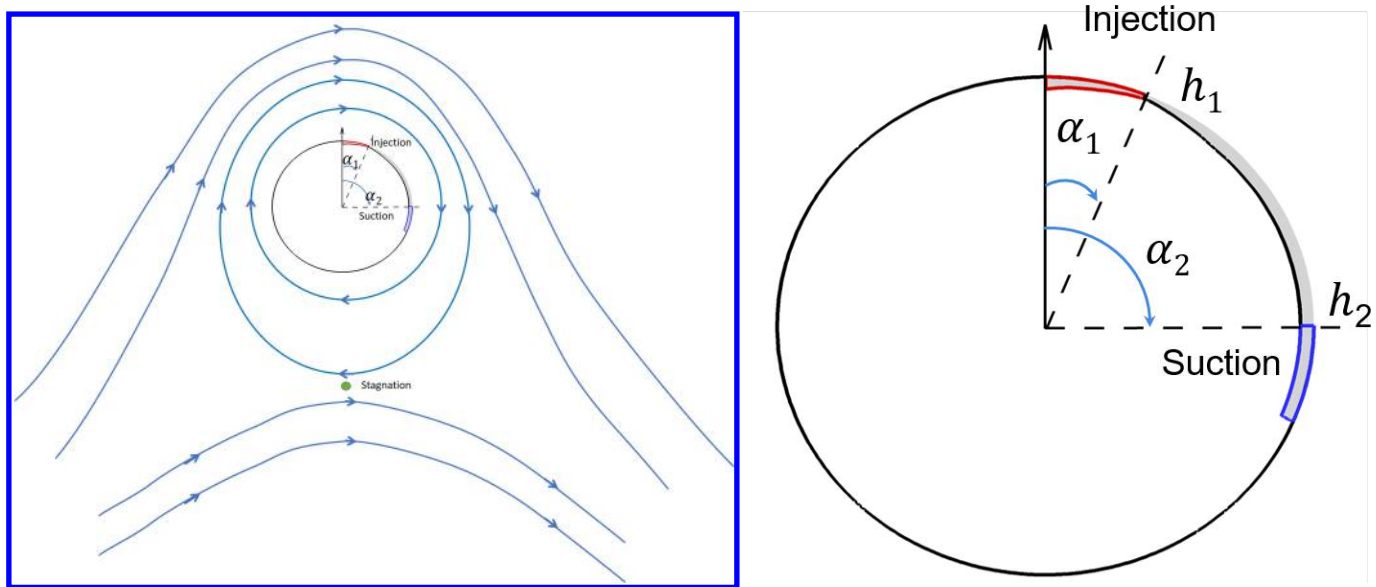


Figure 7: CFJ flow control illustration on circular cylinder

From the potential flow theory, to achieve the super-lift coefficient, the flow stagnation point should be detached from the surface as shown in flow field in Fig. 7. However, for a circular cylinder, the vortex shedding usually starts near the very top and bottom points and forms a large wake behind the cylinder. The intuition is thus to apply the CFJ on the downstream side of the cylinder near the very top and bottom point to remove flow separation by energizing the wake flow. The geometry parameters for CFJ flow control on cylinder are hence defined as injection slot location α_1 and slot size h_1 and suction slot location α_2 and slot size h_2 as illustrate in Fig. 7. Please note that the slot location angle is measured from y-axis. If $\alpha_1 = 0$, it means the injection slot is located at the very top position. Table 1 shows several CFJ cylinder geometries with varied geometry parameters for trade study. The injection and suction slot size is normalized by the cylinder diameter.

Table 1: Geometry parameters for the CFJ cylinder.

Cases	Injection slot location $\alpha_1(^{\circ})$	Injection slot size (%)	Suction slot location $\alpha_2(^{\circ})$	Suction slot size (%)
1	0	0.125	90	1
2	0	0.125	135	1
3	0	0.125	180	1
4	15	0.125	135	1
5	-15	0.125	135	1
6	0	0.25	135	1
7	0	0.5	135	1
8	0	0.125	135	0.5
9	0	0.125	135	2

The 2D structured meshes are constructed using the O-mesh topology in order to achieve high mesh quality on cylinder surface. A total of 1601 grid points are placed around the cylinder and 121 points normal to the wall surface with an additional 41 grid points across the jet slot. The total mesh size is 216,000 cells, and is partitioned into 7 blocks for parallel computation. The farfield boundary is located about 60 reference length (diameter) away from the cylinder. To resolve the turbulent boundary layer, the first grid point is placed at $y^+ \approx 1$. The block information is found in Table 2 and the mesh topology is shown in Fig. 8.

Table 2: Grid size distribution CFJ cylinder

Block	ξ -Direction	η -Direction	Cell number	location
1-4	401	121	48000	around the cylinder
5	101	41	4000	Injection block
6	401	41	16000	Connection
7	101	41	4000	Suction block
Total mesh size			216000	

5 Results and Discussion

5.1 Validation of Computational code

The numerical investigation of stationary circular cylinder at the Reynolds number of $Re = 3.03 \times 10^6$ is conducted to validate the computational code. The pressure coefficient C_p are plotted with the azimuth angle in

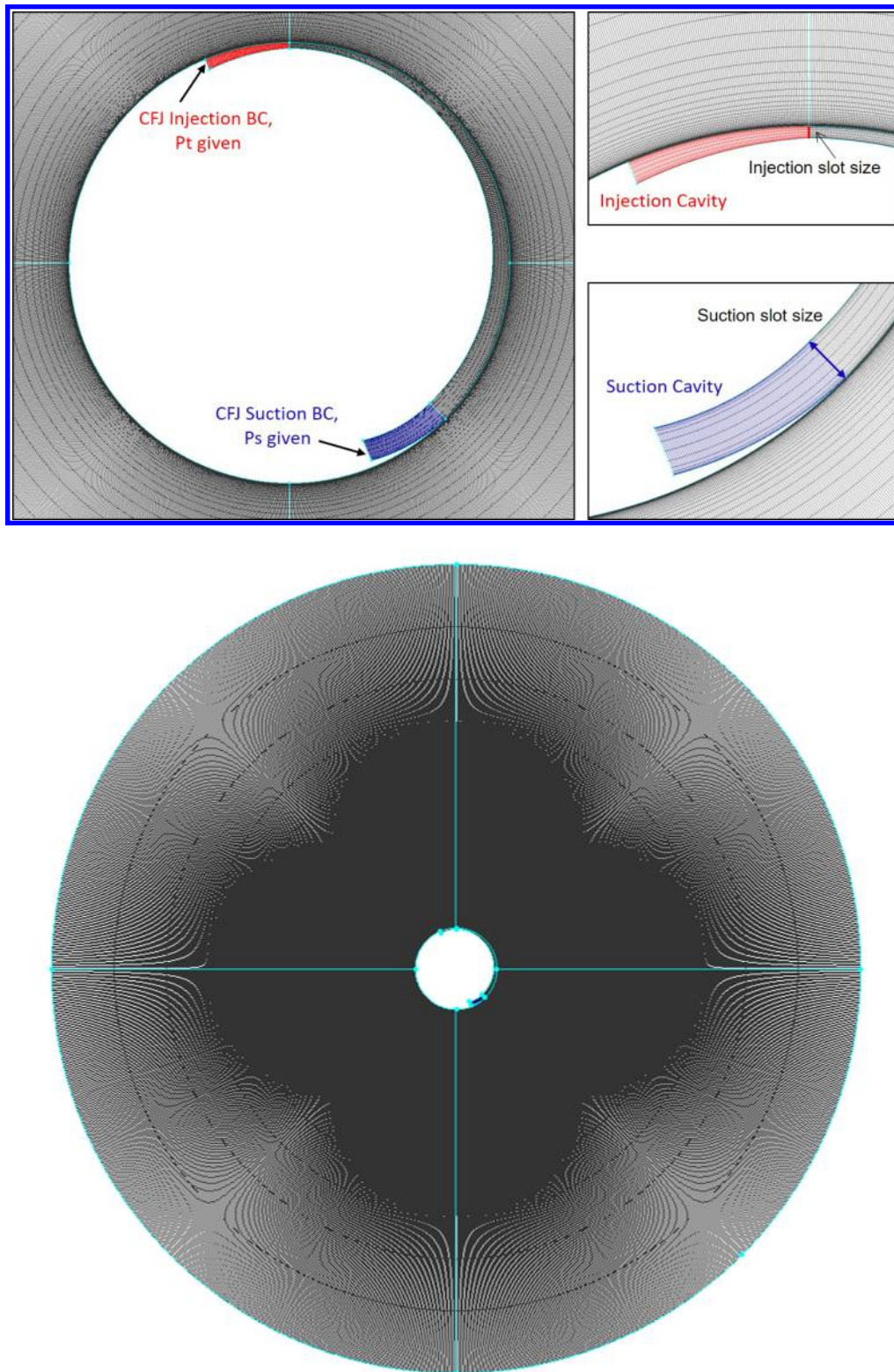


Figure 8: Computational mesh for CFJ cylinder calculation.

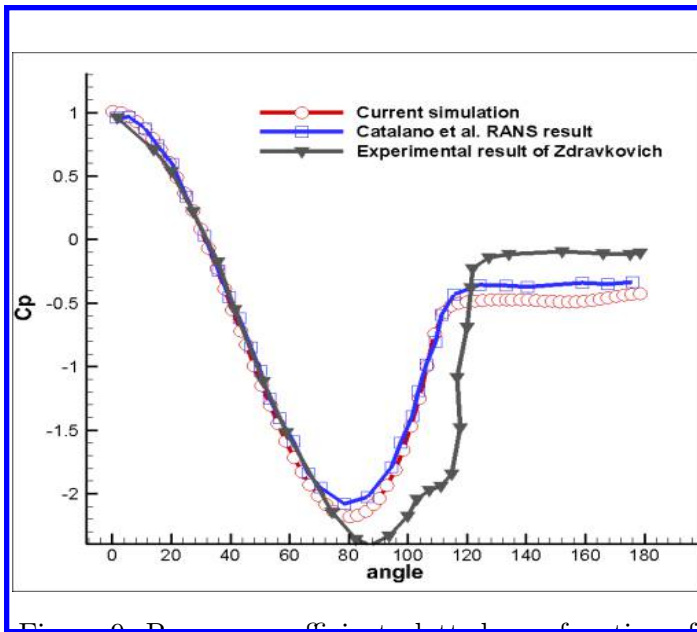


Figure 9. Pressure coefficient plotted as a function of the azimuth angle for one semi-circle of the cylinders surface

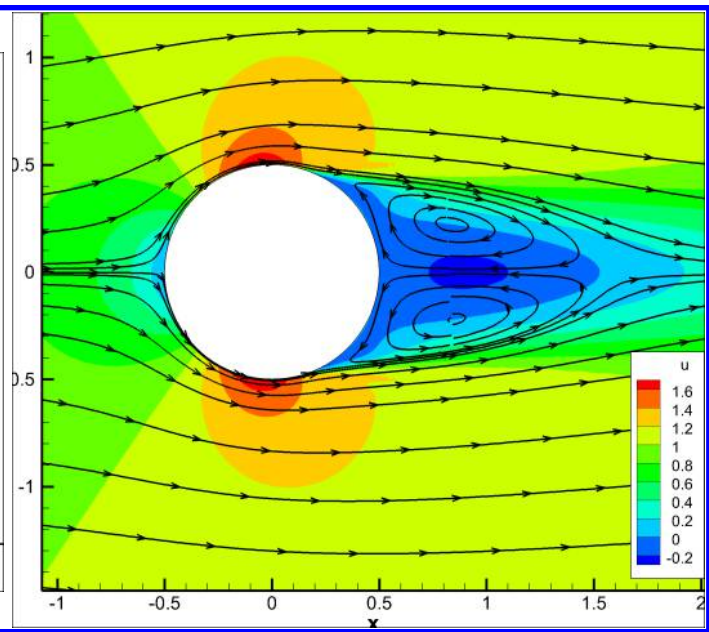


Figure 10: streamlines of steady state RANS results for the stationary cylinder flow

Fig. 9. The relevant experimental results are available at Re near 1×10^6 . The steady RANS simulation predicted results agrees well with the experiment with some deviation. The deviation is due to the intrinsic feature of RANS simulation, which filters unsteady and turbulent flow energy. The streamlines are given in Fig. 10.

5.2 CFJ Cylinder Trade Study

In this section, a parametric trade study is conducted to evaluate the influence of the CFJ airfoil geometry parameters, including the suction slot size h_2 , suction location α_1 , injection slot size h_1 , and injection location α_1 . The flow simulation parameters are as listed in table 3. For the CFD simulation, the Mach number of 0.063 and Reynolds number of 3.03 million are used.

Table 3: CFD simulation parameters

Mach number	Reynolds number	C_μ
0.063	3,030,000	0.2-0.8

5.2.1 Suction Location

Three suction slot locations are used, 90° , 135° , and 180° . The jet momentum coefficients C_μ varies from 0.2 to 0.8. The case 1, 2 and 3 in Table 1 are described in this section with the injection slot fixed at 0° location.

Fig. 11 shows the computed lift and drag coefficients with different jet momentum coefficients. The lift coefficient increases with C_μ for all three configurations with different suction slot locations. For the same C_μ , the lift coefficient is higher for the suction location of $\alpha_2 = 135^\circ$. For all the three configurations, the lift coefficient is greater than 15.0 when C_μ is greater than 0.7. When C_μ is 0.8, both the suction location at 90° and 135° reach

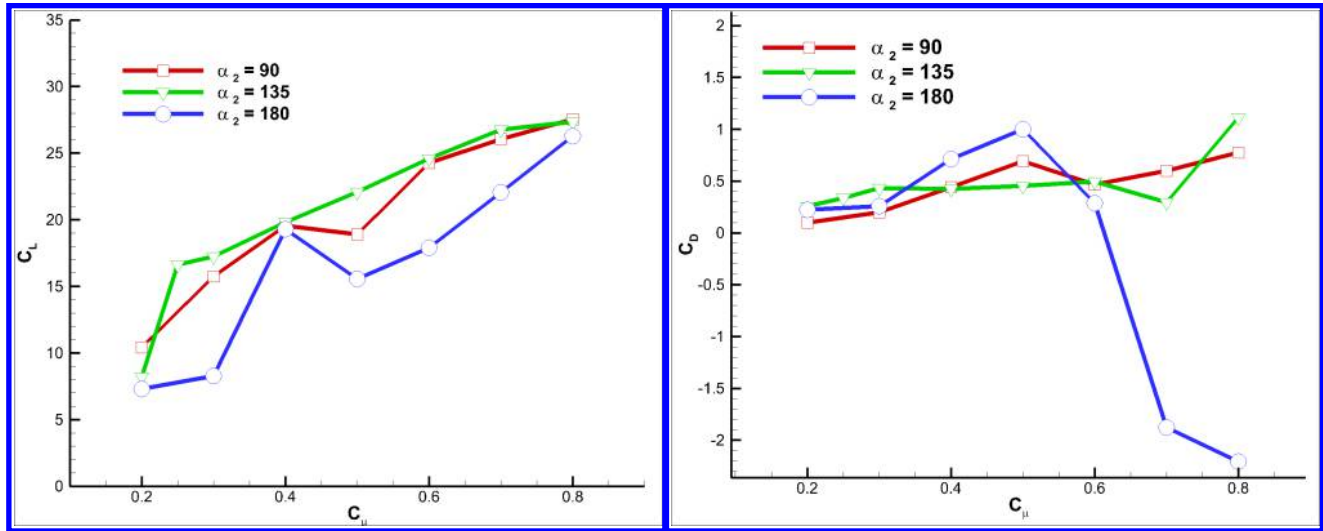


Figure 11: Lift and drag coefficient vs C_μ for the cylinder with CFJ flow control at different suction locations.

the C_L of 28. The suction location at 180° has the C_L slightly lower with the value of 27. The maximum lift coefficients for the CFJ cylinder at $\alpha_2 = 135^\circ$ are increased dramatically to 28 at $C_\mu = 0.8$. Obviously, the lift coefficient of CFJ cylinder easily exceeds the theoretical limit of $4\pi = 12.56$ by far.

The drag coefficients of the CFJ cylinder are largely varied with the suction slot location. The negative drag coefficient is the thrust created by the CFJ power introduction. For the suction slot location at $\alpha_2 = 180^\circ$, a very large thrust (negative drag) is generated attributed to the horizontal placement of the suction slot, which generates all the suction impulse in the thrust direction as shown in Eq. (1). Since the injection slot is located at the 0° location for all the cases studied in this section, the injection jet has all the impulse always in the thrust direction.

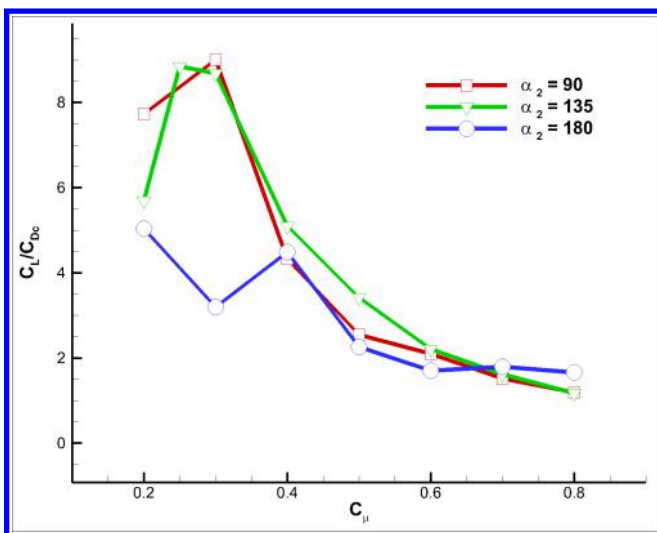


Figure 12: Aerodynamic efficiency C_L/C_{Dc} versus C_μ

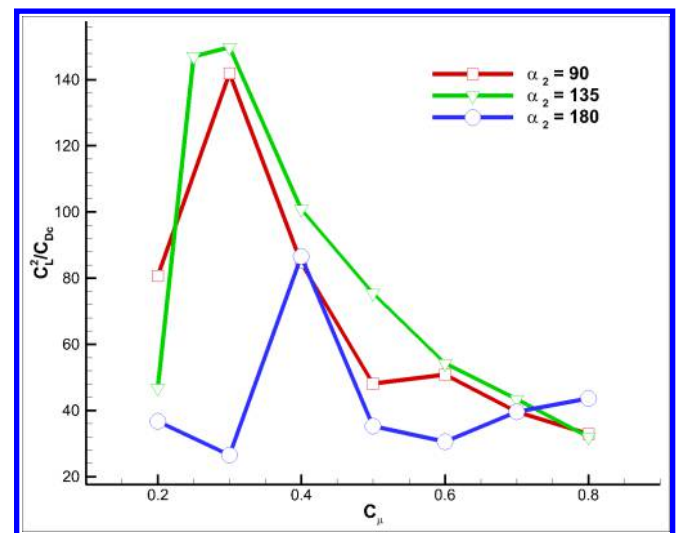


Figure 13: Productivity efficiency C_L^2/C_{Dc} versus C_μ

For the corrected aerodynamic efficiency C_L/C_{Dc} in Fig. 12, a CFJ cylinder has comparatively high values for

such high lift coefficients. The maximum value of $C_L/C_{Dc} = 6.0$ is obtained at $C_\mu = 0.4$ with the suction slot location of $\alpha_2 = 135^\circ$. The lift coefficient of 19.5 is obtained at the best efficiency point. At high C_μ , since the flow can not absorb more energy and the flow in the suction slot becomes choked, the higher C_μ will decrease the aerodynamic efficiency. The high lift contribution to the productivity efficiency is reflected by C_L^2/C_D in Fig. 13. The maximum productivity efficiency of about 155 is obtained by the suction location at 135° and C_μ of 0.3.

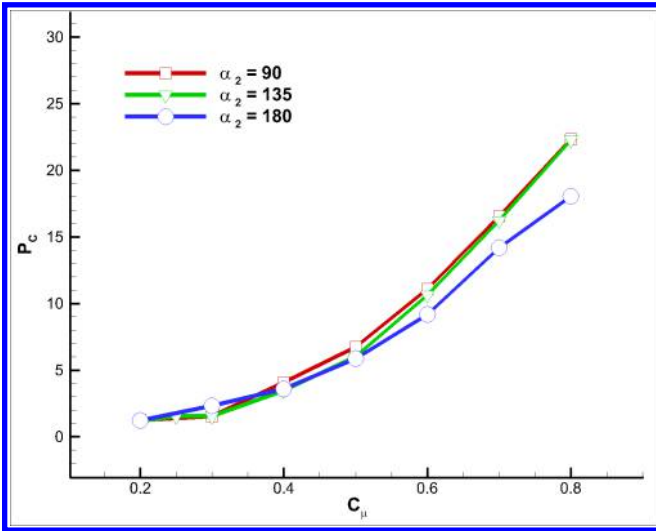


Figure 14: Power coefficient C_L vs C_μ

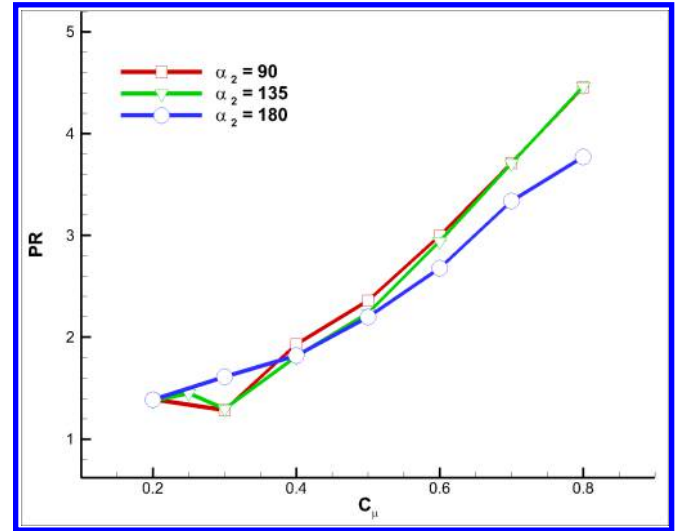


Figure 15: Pressure ratio PR vs C_μ

The power coefficients of the CFJ pumping are calculated based on Eq. (7) and (8) using a constant pumping efficiency value of 100%. The results are shown in Fig. 14. The power coefficient increase rapidly with C_μ . Fig. 15 is the total pressure ratio PR calculated by the ratio of the total pressures at the injection and suction cavity. The CFJ pumping power is largely determined by the total pressure ratio PR between the injection and suction cavity. The total pressure ratio PR has a similar variation trend to the power coefficient with the injection jet momentum coefficient.

Flow Structures

Fig. 16 displays a qualitative comparison of the streamlines and Mach number contours at different jet momentum coefficient C_μ at the suction location of $\alpha_2 = 135^\circ$. At the lower jet momentum coefficient $C_\mu = 0.2$, there are two stagnation points attached on the solid surface (see Fig. 16(a)). Both the upstream and downstream stagnation points are located at the lower surface of cylinder. The flow pattern represents the small circulation introduced in the flow. The downstream stagnation point is observed near the suction slot, where the flow from the lower surface and the upper surface collides. The flow direction is changed drastically around the second stagnation point with the reversed flow from the lower surface near the suction slot (see Fig. 16(b)). As the jet momentum coefficient is increased and the jet becomes larger, the two stagnation points are merged and form the single stagnation point detached from the solid surface (see Fig. 16(c-d)). Increasing the jet momentum coefficient drives the stagnation point further away from the cylinder.

For all three suction configurations of Case 1, 2, and 3 at $C_\mu = 0.3$, the Mach contours and streamlines are shown in Fig. 17. With the CFJ jet flow mixing, the flow field is fully attached to the surface and creates very large circulation around the cylinder surface. The stagnation point is far detached from the solid surface. The upstream incoming flow follows front cylinder surface, turns around the top surface by 180° , and is nicely attached to the rear surface due to the strong induction effect from the high momentum co-flow jet. Note that the stagnation point location is a little different for three different suction slot locations. For $\alpha_2 = 135^\circ$, the stagnation point is

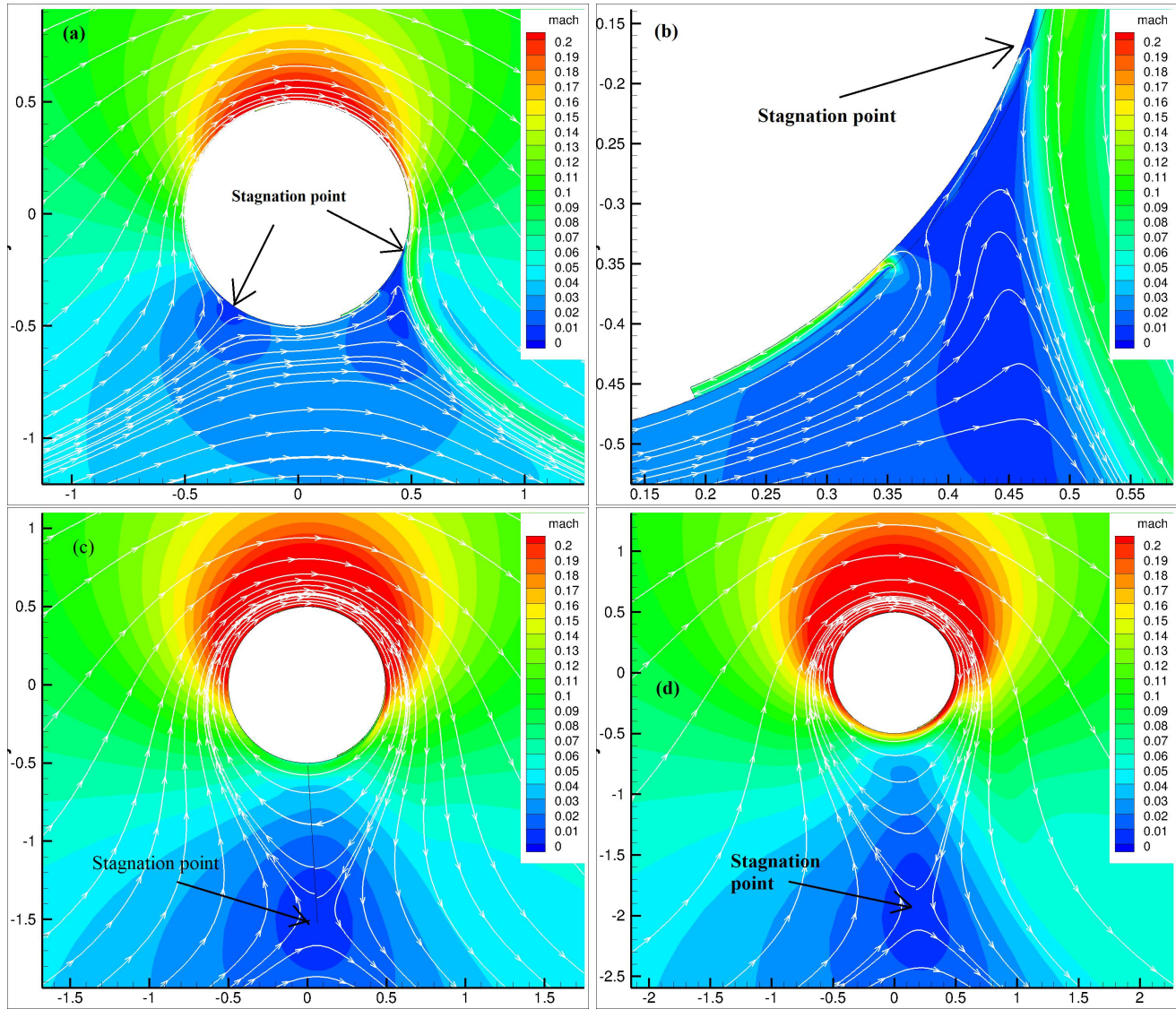


Figure 16: The Mach number and streamlines at the jet momentum coefficient C_μ of 0.2, 0.3 and 0.5

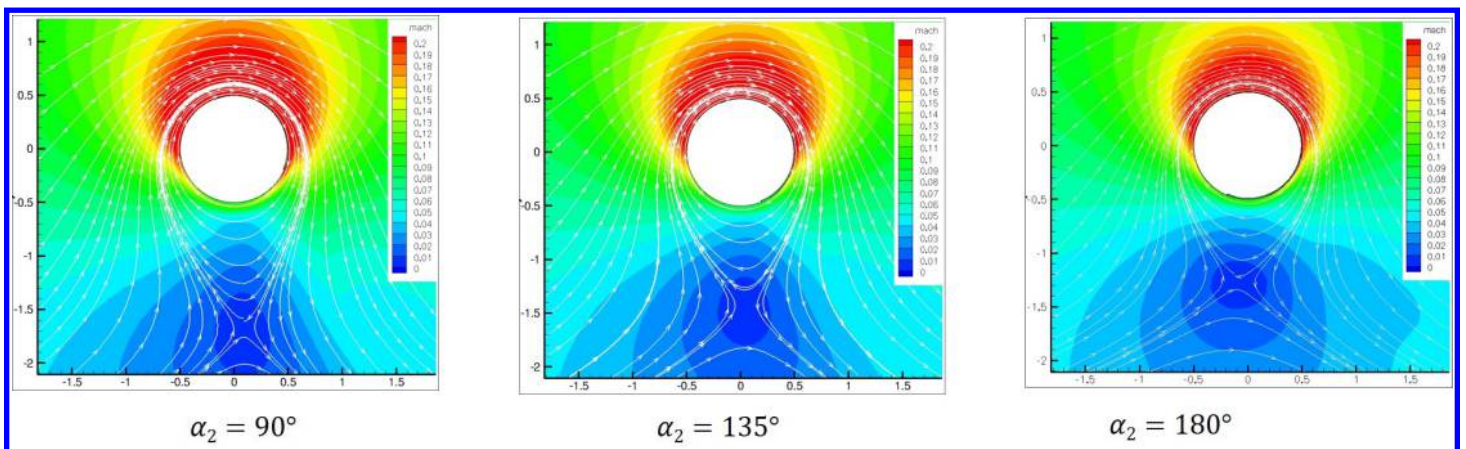


Figure 17: Mach contours and streamlines at $C_\mu = 0.6$

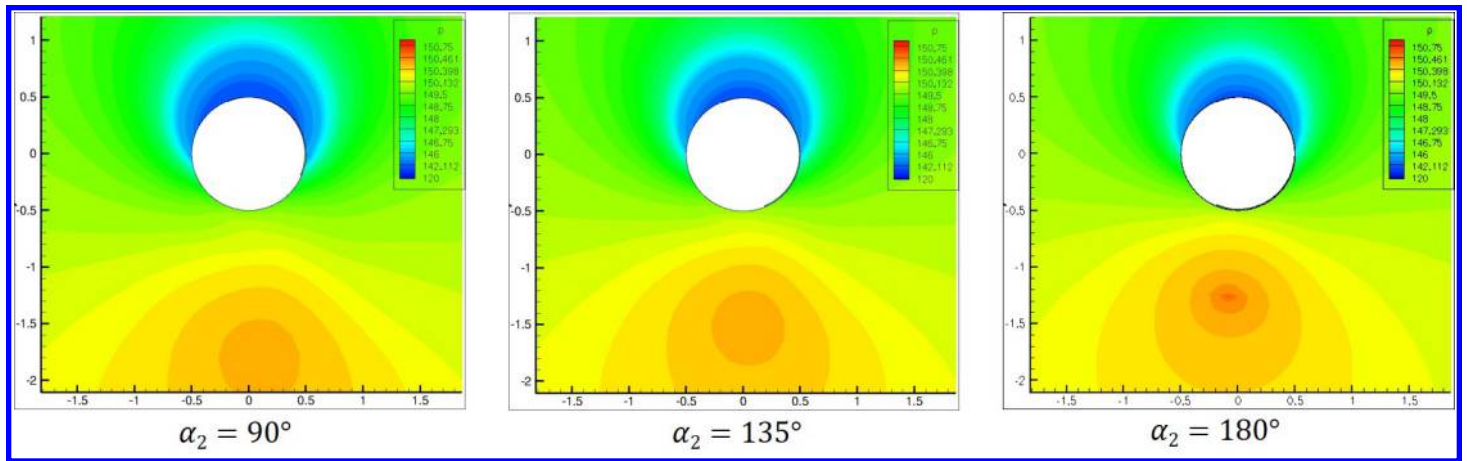


Figure 18: Pressure distribution at different suction configurations

located exactly on the y -axis below the cylinder at the length of 1.5 diameter and $x_{stagnation} = 0$ (the middle plot of Fig. 17). When the suction slot is located at the lowest point of the cylinder at $\alpha_2 = 180^\circ$, the stagnation point is shifted upstream to $x_{stagnation} = -0.15$. For the suction slot located at $\alpha_2 = 90^\circ$, the stagnation point shifts downstream to $x_{stagnation} = 0.15$ (the right plot of Fig. 17). This flow stagnation point is driven by the suction slot location by its suction effect. For $\alpha_2 = 180^\circ$, higher suction force is required to make the flow turn 180° . Therefore, the resulting flow field will shift the stagnation point upstream.

Fig. 18 shows the computed static pressure contour for the CFJ cylinder at different suction locations. At the top of the cylinder, the super-suction effect is generated with a very low static pressure. Near the bottom of the cylinder, the high pressure regions are obtained by the stagnation areas. The pressure field is almost symmetric about the y -axis for the suction slot located at 135° , which provides slightly highest lift coefficient at $C_\mu = 0.3$ as shown in Fig. 11.

5.2.2 Suction Slot Size

Fig. 19 is the comparison of lift and drag coefficients among the different suction slot sizes of CFJ flow control cylinder. The baseline CFJ cylinder has a suction size of 2%. The increased suction slot size has a negative effect of lift enhancement at higher $C_\mu > 0.3$. At the lower value of C_μ , the lift coefficient is higher for larger suction slot size. For the drag coefficient, the 4% slot size has a large variation with negative drag at low C_μ and a rapid increase to large positive drag at high C_μ . The 2% slot size is fairly stable with a positive drag at different C_μ .

5.2.3 Injection Location

Fig. 20 presents the lift and drag coefficients with different injection slot locations. It is obvious that when we move the injection slot away from the very top location, the lift coefficient is reduced and the drag coefficient is increased.

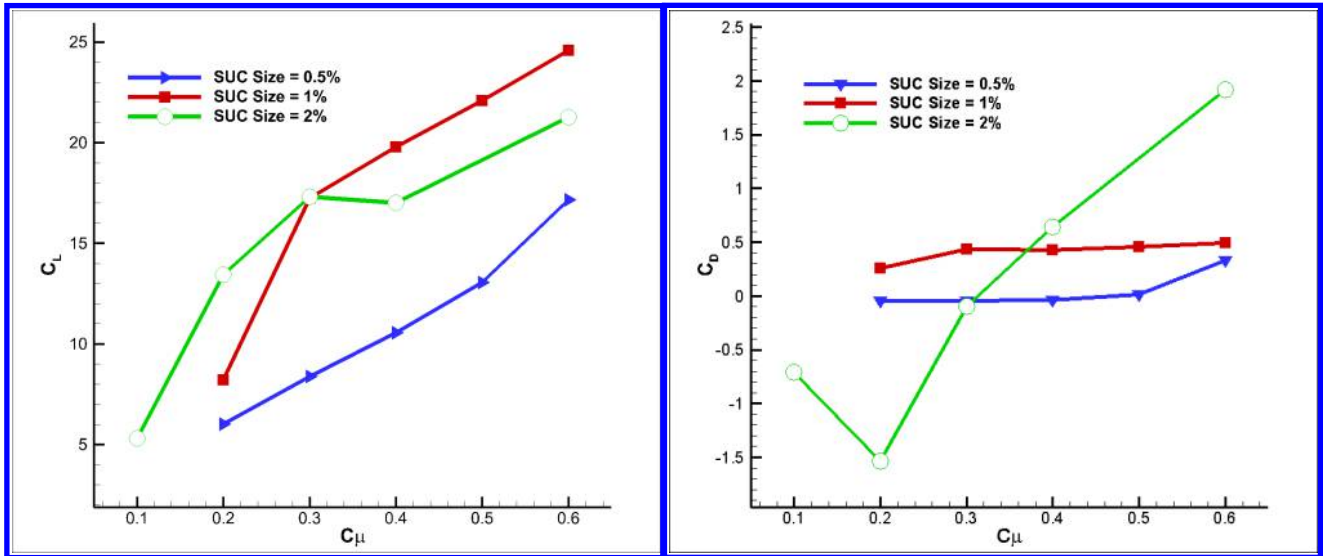


Figure 19: Lift and drag coefficient with different suction slot sizes

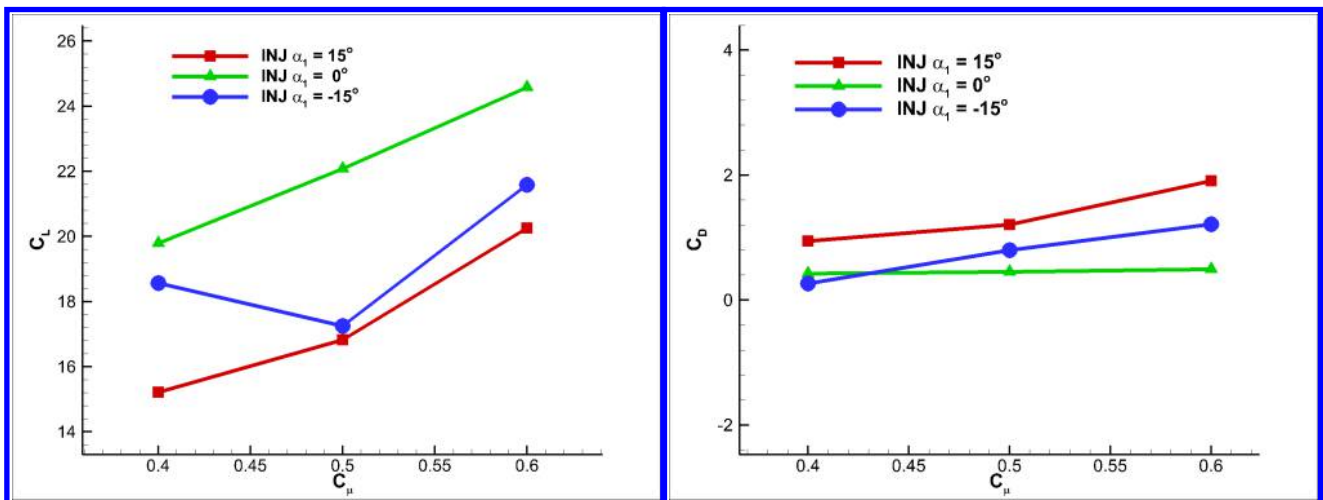


Figure 20: Lift and drag coefficient with different injection location

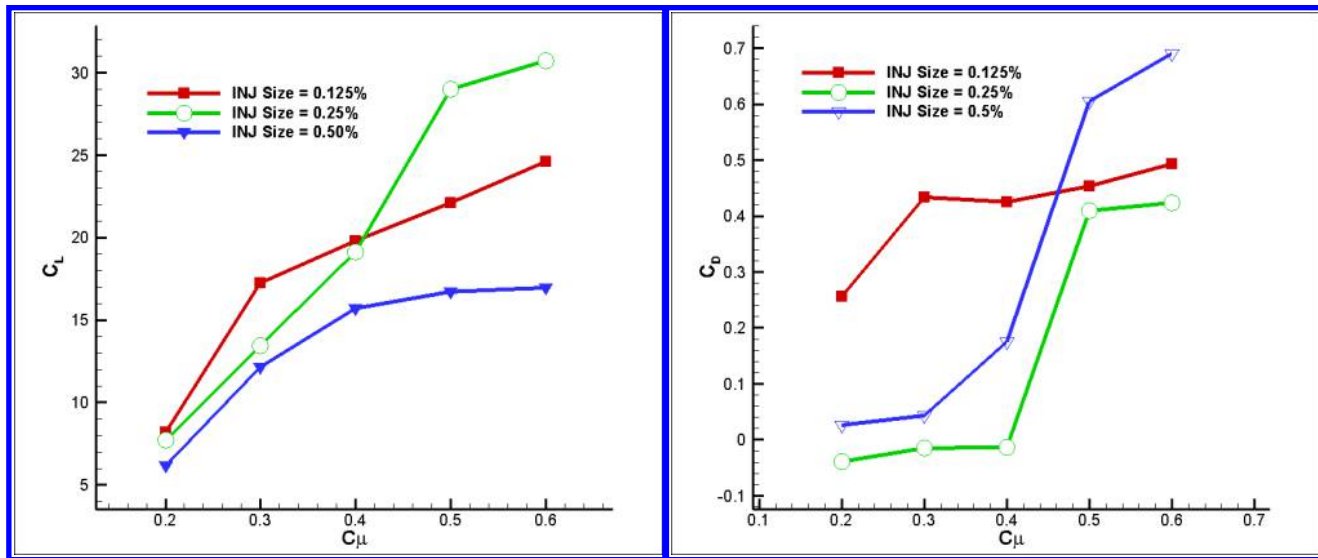


Figure 21: Lift and drag coefficients with different injection slot sizes

5.2.4 Injection Slot Size

Fig. 21 is the simulation results of different injection slot size. It is shown that when the injection slot size is decreased, the lift coefficient is increased at lower C_{μ} . At higher C_{μ} , reducing the injection slot size will decrease the lift coefficient. The increased slot size has substantially lower drag.

6 Conclusion

This paper investigates the maximum lift coefficient for Co-Flow Jet flow control on cylinder flows. The numerical study indicates that CFJ flow control is able to achieve the maximum lift coefficient far exceeding the theoretical limit. Several CFJ cylinder configurations are created for parametric trade study. The best lift coefficient with highest efficiency is obtained at the suction slot location at and injection slot location at 0° . The injection slot location of 0° appears to be the optimum for all the aerodynamic and efficiency performance. The maximum lift coefficient of $C_L=28$ is achieved at $C_{\mu} = 0.8$.

7 Acknowledgment

This project is sponsored by the Defense Advanced Research Projects Agency and monitored by the program manager Jean-Charles Ledé under Cooperative Agreement No.: HR0011-16-2-0052. The content of the information does not necessarily reflect the position or the policy of the Government, and no official endorsement should be inferred. The simulations are conducted on Pegasus supercomputing system at the Center for Computational Sciences at the University of Miami. More detailed qualitative and quantitative analysis of simulation results will be presented in the full paper.

References

- [1] T. O. G. Prandtl, Ludwig, *Applied Hydro- and Aeromechanics (Dover Books on Aeronautical Engineering)*. Dover Publications, 1934.
- [2] P. Tokumar and P. Dimotakis, “The lift of a cylinder executing rotary motions in a uniform flow,” *Journal of Fluid Mechanics*, vol. 255, pp. 1–10, 1993.
- [3] S. Mittal and B. Kumar, “Flow past a rotating cylinder,” *Journal of Fluid Mechanics*, vol. 476, pp. 303–334, 2003.
- [4] S. Kumar, C. Cantu, and B. Gonzalez, “Flow past a rotating cylinder at low and high rotation rates,” *Journal of Fluids Engineering*, vol. 133, no. 4, p. 041201, 2011.
- [5] S. Karabelas, B. Koumroglou, C. Argyropoulos, and N. Markatos, “High reynolds number turbulent flow past a rotating cylinder,” *Applied mathematical modelling*, vol. 36, no. 1, pp. 379–398, 2012.
- [6] J. D. Brooks, “The effect of a rotating cylinder at the leading and trailing edges of a hydrofoil,” tech. rep., NAVAL ORDNANCE TEST STATION CHINA LAKE CA, 1963.
- [7] A. Alvarez-Calderon, “High lift and control system for aircraft,” July 7 1964. US Patent 3,140,065.
- [8] J. Seifert, “A review of the magnus effect in aeronautics,” *Progress in Aerospace Sciences*, vol. 55, pp. 17–45, 2012.
- [9] Y. Zhuang, X. Sun, D. Huang, and G. Wu, “Numerical study on aerodynamic performances of the wind turbine rotor with leading-edge rotation,” *Journal of Renewable and Sustainable Energy*, vol. 4, no. 6, p. 063103, 2012.
- [10] V. Modi, “Moving surface boundary-layer control: A review,” *Journal of fluids and structures*, vol. 11, no. 6, pp. 627–663, 1997.
- [11] J. D. Anderson Jr, *Fundamentals of aerodynamics*. Tata McGraw-Hill Education, 2010.
- [12] V. E. Lockwood, *Lift generation on a circular cylinder by tangential blowing from surface slots*. National Aeronautics and Space Administration, 1960.
- [13] G.-C. Zha, W. Gao, and C. Paxton, “Jet Effects on Co-Flow Jet Airfoil Performance,” *AIAA Journal*, No. 6., vol. 45, pp. 1222–1231, 2007.
- [14] G.-C. Zha and D. C. Paxton, “A Novel Flow Control Method for Airfoil Performance Enhancement Using Co-Flow Jet.” *Applications of Circulation Control Technologies*, Chapter 10, p. 293-314, Vol. 214, Progress in Astronautics and Aeronautics, AIAA Book Series, Editors: Joslin, R. D. and Jones, G.S., 2006.
- [15] G.-C. Zha, C. Paxton, A. Conley, A. Wells, and B. Carroll, “Effect of Injection Slot Size on High Performance Co-Flow Jet Airfoil,” *AIAA Journal of Aircraft*, vol. 43, 2006.
- [16] G.-C. Zha, B. Carroll, C. Paxton, A. Conley, and A. Wells, “High Performance Airfoil with Co-Flow Jet Flow Control,” *AIAA Journal*, vol. 45, 2007.
- [17] Wang, B.-Y. and Haddoukessouni, B. and Levy, J. and Zha, G.-C., “Numerical Investigations of Injection Slot Size Effect on the Performance of Co-Flow Jet Airfoil ,” *AIAA Journal of Aircraft*, vol. 45, pp. 2084–2091, 2008.

- [18] B. P. E. Dano, D. Kirk, and G.-C. Zha, “Experimental Investigation of Jet Mixing Mechanism of Co- Flow Jet Airfoil.” AIAA-2010-4421, 5th AIAA Flow Control Conference, Chicago, IL, 28 Jun - 1 Jul 2010.
- [19] B. P. E. Dano, G.-C. Zha, and M. Castillo, “Experimental Study of Co-Flow Jet Airfoil Performance Enhancement Using Micro Discreet Jets.” AIAA Paper 2011-0941, 49th AIAA Aerospace Sciences Meeting, Orlando, FL, 4-7 January 2011.
- [20] Lefebvre, A. and Zha, G.-C. , “Design of High Wing Loading Compact Electric Airplane Utilizing Co-Flow Jet Flow Control.” AIAA Paper 2015-0772, AIAA SciTech2015: 53rd Aerospace Sciences Meeting, Kissimmee, FL, 5-9 Jan 2015.
- [21] Lefebvre, A. and Dano, B. and Bartow, W. and Di Franzo, M. and Zha, G.-C., “Performance Enhancement and Energy Expenditure of Co-Flow Jet Airfoil with Variation of Mach Number.” AIAA Paper 2013-0490, AIAA Journal of Aircraft, DOI: 10.2514/1.C033113, 2016.
- [22] Liu, Z.-X. and Zha, G.-C., “Transonic Airfoil Performance Enhancement Using Co-Flow Jet Active Flow Control.” AIAA Paper 2016-3066, AIAA Aviation, June 13-17 2016.
- [23] Yunchao Yang and Gecheng Zha, “Super-Lift Coefficient of Active Flow Control Airfoil: What is the Limit?.” AIAA Paper 2017-1693, AIAA SCITECH2017, 55th AIAA Aerospace Science Meeting, Grapevine, January 9-13 2017.
- [24] Lefebvre, A. and Zha, G.-C., “Trade Study of 3D Co-Flow Jet Wing for Cruise Performance.” AIAA Paper 2016-0570, AIAA SCITECH2016, AIAA Aerospace Science Meeting, San Diego, CA, 4-8 January 2016.
- [25] P. R. Spalart and S. R. Allmaras, “A one-equation turbulence model for aerodynamic flows,” in *30th Aerospace Sciences Meeting and Exhibit, Aerospace Sciences Meetings, Reno, NV, USA, AIAA Paper 92-0439*, 1992.
- [26] Y.-Q. Shen and G.-C. Zha, “Large Eddy Simulation Using a New Set of Sixth Order Schemes for Compressible Viscous Terms ,” *Journal of Computational Physics*, vol. 229, pp. 8296–8312, 2010.
- [27] Zha, G.C., Shen, Y.Q. and Wang, B.Y., “An improved low diffusion E-CUSP upwind scheme ,” *Journal of Computer and Fluids*, vol. 48, pp. 214–220, Sep. 2011.
- [28] Y.-Q. Shen and G.-Z. Zha , “Generalized finite compact difference scheme for shock/complex flowfield interaction,” *Journal of Computational Physics*, vol. doi:10.1016/j.jcp.2011.01.039, 2011.
- [29] Shen, Y.-Q. and Zha, G.-C. and Wang, B.-Y., “Improvement of Stability and Accuracy of Implicit WENO Scheme,” *AIAA Journal*, vol. 47, No. 2, pp. 331–344, 2009.
- [30] Shen, Y.-Q. and Zha, G.-C. and Chen, X.-Y., “High Order Conservative Differencing for Viscous Terms and the Application to Vortex-Induced Vibration Flows,” *Journal of Computational Physics*, vol. 228(2), pp. 8283–8300, 2009.
- [31] Shen, Y.-Q. and Zha, G.-C. , “Improvement of the WENO Scheme Smoothness Estimator,” *International Journal for Numerical Methods in Fluids*, vol. DOI:10.1002/fld.2186, 2009.
- [32] G.-C. Zha and E. Bilgen, “Numerical Study of Three-Dimensional Transonic Flows Using Unfactored Upwind-Relaxation Sweeping Algorithm,” *Journal of Computational Physics*, vol. 125, pp. 425–433, 1996.
- [33] B.-Y. Wang and G.-C. Zha, “A General Sub-Domain Boundary Mapping Procedure For Structured Grid CFD Parallel Computation,” *AIAA Journal of Aerospace Computing, Information, and Communication*, vol. 5, No.11, pp. 2084–2091, 2008.

- [34] Wang, B. Y and Zha, G.-C. , “Detached-Eddy Simulation of a Co-Flow Jet Airfoil at High Angle of Attack.” AIAA Paper 2009-4015, accepted for publication in *Journal of Aircraft*, 2011.
- [35] Im, H.-S. and Zha, G.-C. and Dano, B. P. E., “Large Eddy Simulation of Coflow Jet Airfoil at High Angle of Attack,” *Journal of Fluid Engineering*, vol. 136(2), p. 021101, 2014.
- [36] Y.-Q. Shen, G.-C. Zha, and B.-Y. Wang, “Improvement of Stability and Accuracy of Implicit WENO Scheme ,” *AIAA Journal*, vol. 47, pp. 331–344, 2009.